Shear failure and fracturing of horizontally layered shale

Marte Gutierrez
Colorado School of Mines, Golden, CO, USA

Daisuke Katsuki
Colorado School of Mines, Golden, CO, USA

Runar Nygaard
Oklahoma University, Norman, OK, USA

ABSTRACT: Understanding the mechanical behavior of shale formations is becoming increasingly important. Shales are essential in oil and gas production from tight unconventional resources. In geological carbon sequestration of CO_2, shales typically form the caprock for geological storage. Fractures provide high permeability pathways for fluid flow and leakage for shales because of their low permeability. Shales have a layered structure with discontinuities parallel to the bedding plane, which can result in distinct anisotropy in their hydro-mechanical behavior. This paper aims to understand better the effects of intrinsic structural anisotropy from their layered structure on shale shear failure and fracturing behavior. Triaxial shear tests at constant confining stress were conducted on shale samples drilled horizontally parallel to the bedding plane. A new mechanism is proposed to explain the formation of shear/extensional fractures along bedding planes when shale samples are sheared under significant constant confining stress with the major principal stress perpendicular to the bedding plane.

Keywords: Bedding planes, Layering, Shear Failure, Fracturing, Leakage.

1 INTRODUCTION

Shales are the most ubiquitous materials in the Earth's regolith. Shales typically have very low permeability ranging from pico- to micro-Darcy (e.g., Neuzil 1994) due to their very tight matrices mainly composed of kerogen, other organic matter, clay minerals, and silica. Shales are acknowledged to play essential roles in geo-energy and geo-environmental applications. Shale oil and gas are promising hydrocarbon resources. Due to their very low permeability, economic shale gas/oil production is only possible by hydraulic fracturing of the shale. Also, due to their low permeability, shales are a common cap rock layer for CO_2 sequestration in geological reservoirs such as deep saline aquifers (IPCC 2005). The caprock layers are expected to physically trap the CO_2 plume in the reservoir for an extended period. The fracturing of caprock shales would allow the sequestered CO_2 to escape to drinking water aquifers or the atmosphere, thereby reducing the effectiveness of geological sequestration. Hydraulic fracturing is the most common form of shale stimulation by increasing the pore pressure until it exceeds the combined minimum effective principal stress and the tensile strength of the rock (Guo et al. 2018). However, shales can also fracture due to shear failure when the shear stress exceeds the shear strength and can also enhance shale permeability. Nevertheless, shear fracturing in shale is less understood than tensile fracturing.

Shales are fine-grained clastic sedimentary rocks that can break into thin layers, usually in the direction parallel to the bedding plane. They are composed of mud, a mixture of clay minerals flakes, and tiny fragments (silt-sized particles) of other minerals, especially quartz and calcite. The main characteristic that differentiates shales from mudrocks is their fissility, making them easy to break

into thin laminae along horizontal layers or bedding planes. Shale microstructure is often strongly anisotropic because of heterogeneities, particularly laminations along the bedding planes. The anisotropic microstructure of shales is widely known. However, there remains a limited understanding of the effects of structural anisotropy on shale mechanical behavior.

2 TEST SAMPLE, APPARATUS, AND PROCEDURES

The test material used in the study was obtained from a block sample of Mancos shale retrieved from Douglas Creek Arch, located between the Uinta and Piceance basins in Colorado, USA. Mancos shale is an organic-rich deposit of the Late Cretaceous age widely found in the Western USA and is considered a rich rock source of oil and gas for unconventional reservoirs horizontal drilling.

Two cylindrical samples were horizontally cored from the block of Mancos shale. Since the samples were drilled horizontally, the bedding planes are parallel to the height of the samples, and the bedding planes are also parallel to the major principal stress σ_1. Fig. 1a and 2a show the triaxial samples before testing, which show well-defined layered microstructure along the bedding plane running from top to bottom. The two cylindrical samples had diameters of 38 mm and heights of about 60 mm and were tested in triaxial loading with constant confining stress σ_3. Drained shear testing of fluid-saturated shales is nearly impossible because of their very low permeability, so the tests are basically undrained. The porosity values are 5.8 and 6.6% for the two triaxial samples.

The two triaxial samples were isotropically consolidated before shearing. After that, the samples were sheared with constant confining pressure σ_3 equal to the consolidation stress. The horizontally cored sample is enclosed in a rubber sleeve and placed in a triaxial core holder. The core holder can apply up to 69 MPa of cell pressure and up to 150 °C of temperature to the sample. To apply the vertical stress σ_1, both ends of the core sample are loaded with axial pistons through grooved metal plates acting as porous stones to distribute compressed air during permeability testing. The cell confining pressure σ_3 is maintained constant at 2 MPa for Sample 1 and 12 MPa for Sample 2 during shearing with a precision ISCO 260D syringe pump. The axial stress of the sample is generated by pushing an axial piston with another ISCO 100DX syringe pump. The piston displacement is measured by using an LVDT whose accuracy is $\pm 0.25\%$ of 1 mm of full scale. The axial displacement is increased while σ_3 is kept constant until the deviatoric or shear stress $(\sigma_1 - \sigma_3)$ reaches the shear strength, and the sample fails and strain-softens to residual stress. The axial strain rate is regulated at 8.1×10^{-3}%/min. Only the axial strain was measured during loading, while the lateral strain was not measured to determine the volumetric change. The triaxial cell was maintained at 80 ºC during the isotropic compression test to reduce the viscosity of the paraffin oil and facilitate pore pressure redistribution in the sample. The Skempton's pore pressure B-parameter is determined to be 0.81, indicating complete saturation given the high stiffness of the sample.

3 TEST RESULTS AND DISCUSSION

After the triaxial tests, the shale core samples were carefully retrieved from the triaxial cell to visually observe and investigate the effect of the confining stress level on the morphology of the induced fractures. Both samples were extensively damaged and developed fractures after shearing. The intact shale sample sheared at constant $\sigma_3 = 2$ MPa and before loading is shown in Fig. 1a. Several wavy/undulating sub-vertical fractures that are highly cemented with calcite span the height of the sample. The lengths of the undulations are in the cm scale above the mm scale, typically associated with larger joint asperities.

Fig. 1b shows a photo of the sample after shearing. Narrow and nearly vertical fractures (highlighted in white lines for clarity) are observed along segments A-A, B-B, and C-C. The major parts of these fractures propagate along the weaker bedding planes of the shale sample. Fig. 1c indicates the fractures observed from the other side of Fig. 1b. The sections from A-A to C-C in this figure correspond to those indicated in Fig. 1b. In addition to these fractures, minor fractures can be observed adjacent to section A-A.

Sample 1 clearly manifested a very brittle response at failure. Remarkably, even at a still significant confining pressure of $\sigma_3 = 2$ MPa, vertical fractures are formed instead of conjugate

shear fractures. Such fractures perpendicular to σ_3 are usually extensional. They typically form due to hydraulic fracturing when the effective minimum principal stress $\sigma_3' = \sigma_3 - u$ becomes negative and exceeds the tensile strength of the rock. However, Sample 1 failed by shearing and not by hydraulic fracturing. As will be shown below, the bedding planes cemented by calcite infill contributed to vertical fracturing.

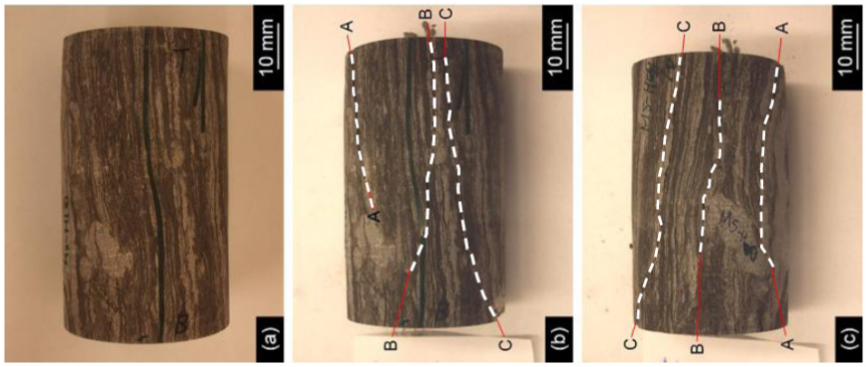

Figure 1. Mancos shale Sample 1 loaded at $\sigma_3 = 2$ MPa. (a) Intact sample, and (b) and (c) Sample after shearing. Sections from A to C indicate the locations of fractures observed externally.

Fig. 2a shows the intact shale sample before shearing at $\sigma_3 = 12$ MPa, and Fig. 2b shows the sample after loading. The sample experienced large deformation, became very short, and significantly bulged laterally after shearing. The sample looked squat after shearing to an axial strain of 20%. The large deformation and bulging indicate very ductile behavior. However, some partially developed conjugated shear cracks are observed close to the sample top and bottom ends, as shown in Fig. 2b (not highlighted because the fractures are clearly visible). These two conjugate shear fractures then created a wedge near both ends resulting in fracturing on two horizontal planes. The sample is placed in the same direction as that of the intact one shown in Fig. 2a. It is seen that the three partial shear fractures were created along sections A-A and B-B. The observed combined distinct bulging and partial shear fracturing of Sample 2 indicate that the sample is in a brittle-to-ductile transition, a rarely observed phenomenon.

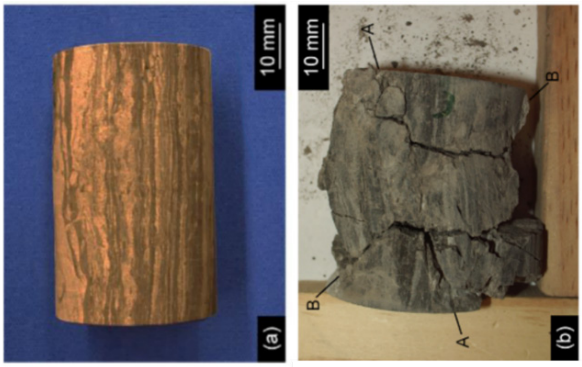

Figure 2. Manacos shale Sample 2 loaded at $\sigma_3 = 12$ MPa. (a) Intact sample and (b) Sample after shearing. Sections from A-A to B-B indicate locations of shear fractures observed externally. The horizontal fractures are due to the wedge created by the conjugate shear fractures.

Fig. 3 shows the Mohr's circles at failure for Samples 1 and 2 plotted in the normal stress σ_n vs. shear stress τ axes. In practice, a minimum of three triaxial tests at different confining stresses are needed to reliably obtain a linear Mohr-Coulomb failure criterion of the following form from the Mohr's circles at failure:

$$\tau = c + \sigma_n tan\phi \tag{1}$$

where ϕ is the friction angle and c is the cohesion. Using only the two triaxial tests, values of c=10.9 and ϕ=45.9° were obtained for Mancos shale, as shown in Fig. 3. Instead of a failure envelope tangent to the two Mohr's circle, a secant friction angle can also be obtained from each test that is tangent to

each Mohr's circle but with an imposed zero cohesion. A secant friction of 75.3° was obtained for Sample 1.

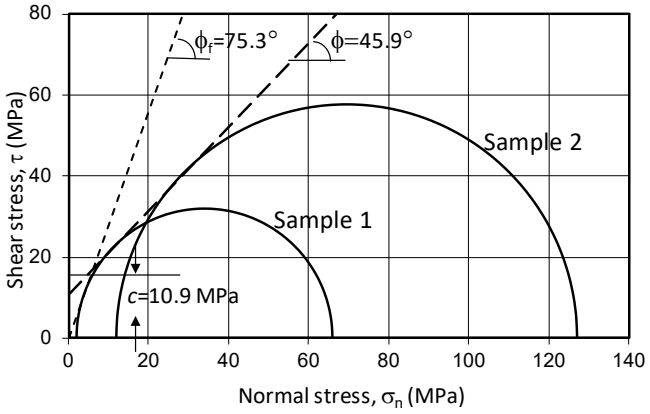

Figure 3. Mohr's circles at failure and failure envelop for the two triaxial tests on Mancos shale. Also shown is the secant friction angle at failure of $\phi_f = 75.3°$ for Sample 1.

As mentioned above, the sub-vertical fractures perpendicular to the minimum principal stress σ_3 for Sample 1 are shown in Figs. 1b and 1c are usually attributed to hydraulic fracturing. However, hydraulic fracturing conditions were not present when test Sample 1 was sheared. Fig. 4 illustrates the postulated mechanism for forming sub-vertical fractures in Sample 1. As shown in Fig. 1 and as idealized in Fig. 4, several undulating bedding planes are observed in Sample 1. Due to the undulations, shear stresses may form along segments of a bedding plane. If these bedding planes are also weak planes, then it is possible for the cementation in the weak planes to fail by shearing and cause the plane to dilate and open. In other words, the bedding planes can be much weaker in shear than the shale matrix, even though the bedding planes are sub-perpendicular to σ_3.

The normal and shear stresses σ_n and τ acting on an undulating segment of the bedding plane can be derived as:

$$\sigma_n = p - qcos(2\alpha)\ ,\ \tau = qsin(2\alpha) \tag{2}$$

where $p = (\sigma_1 + \sigma_3)/2$ is the mean stress, $q = (\sigma_1 - \sigma_3)/2$ is the shear stress, and α is the angle of the local deviation of the undulation from the bedding plane (i.e., the vertical axis). The corresponding mobilized friction ϕ_m acting on an undulating segment of the bedding plane can be calculated as:

$$tan(\phi_m) = \left(\frac{\tau}{\sigma_n}\right) = \frac{sin\phi_f sin(2\alpha)}{1 - cos\phi_f sin(2\alpha)}\ \ ,\ sin(\phi_f) = \left(\frac{q}{p}\right)_f = \left(\frac{\sigma_1 - \sigma_3}{\sigma_1 + \sigma_3}\right)_f \tag{3}$$

where ϕ_f is the friction angle at failure of the intact sample.

Note that the theoretical orientation of the failure surface corresponding to ϕ_f is given as:

$$\alpha_f = 45° - \frac{\phi_f}{2} \tag{4}$$

This equation yields a shear fracture orientation of α=9.32° measured from the vertical axis for the tangent friction angle at failure of 45.9°. This is a low value of the orientation α but still does not yield a vertical fracture with α=0°.

For test Sample 1, the values of the principal stresses at failure were obtained as σ_1=66 MPa and σ_3=2 MPa, giving p=34 MPa and q=32 MPa. Using these values yields ϕ_f=75.3°. For this value, the mobilized friction angle ϕ_m from Eq. (4) can be plotted as a function of α, as shown in Fig. 5. The mobilized friction angle increased up to a peak equivalent to $\phi_m = \phi_f$=75.3°, which was the secant friction angle at failure for Sample 1 (Fig. 3). Because of the high ϕ_m, failure could occur in segments of the undulating bedding deviating less than 5° from the vertical. In fact, a mobilized friction angle of about 30° can be achieved for α of only 1°. Again, the high ϕ_m value for Sample 1 is possible due to the significant difference between σ_1 and σ_3 that is achieved at failure for Sample 1

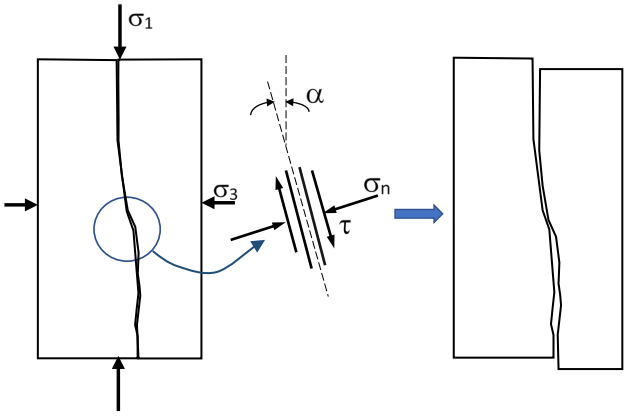

Figure 4. Normal and shear stresses σ_n and τ acting on an undulating bedding plane of a triaxial sample loaded with principal stress σ_1 and σ_3.

In reality, some of the shear stress on the undulation will be carried by the cohesive strength of the bedding plane as explained below. For other friction angles at failure of ϕ_f of 45, 30, and 20°, the maximum mobilized failure occurs at $\phi_m = \phi_f$ and at an angle α_f given in Eq. (4). At α=10°, ϕ_m =35.8 and 17.9 for ϕ_f of 45 and 30°, respectively. Fig. 5 indicates that high mobilized friction angles can be obtained at low undulation angles for typical friction angles at failure of 30 and 45°.

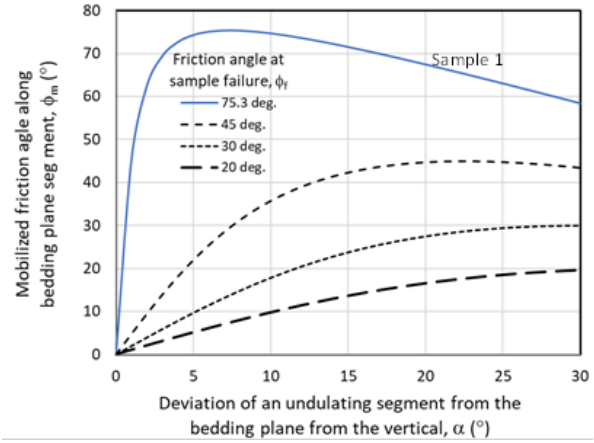

Figure 5. Mobilized friction angle ϕ_m acting on an undulating segment of the bedding plane oriented at α from the vertical with σ_1=66 and σ_3=2 MPa.

Even in the presence of cohesion, a high mobilized friction angle ϕ_m on an undulating segment of the bedding plane can still exceed the shear resistance of the infilled segment and cause shear failure and for the bedding plane to open due to dilation and create a local extensional regime. In the case of the tested Mancos shale, the bedding planes were found to be cemented by calcite infill. Zhao et al. (2022) showed that the linear Mohr-Coulomb failure criterion in Eq. (4) could be employed to describe the shear strength of calcite infilled fractures. Using direct shear tests on fractures infilled with cemented calcite, they obtained a cohesion of c=11.68 MPa and friction angle of ϕ=18.26°.

The failure envelope corresponding to the c and ϕ values from Zhao et al. (2022) is plotted in Fig. 6. Superimposed on the failure envelope are combinations of normal and shear stresses σ_n and τ acting on an undulating segment of the bedding plane with increasing orientation angle α. As can be seen, failure occurs for α of about 12.5° where the stresses σ_n and τ fall on the failure envelope. For Sample 1, the maximum undulations are at about 15°. This result means that localized shear failure of the infilled bedding plan has indeed occurred, causing the sub-vertical fractures shown in Figs. 1b and c. Once the undulating segment of the bedding plane fails, the entire length of bedding planes fails and opens extensionally due to dilation.

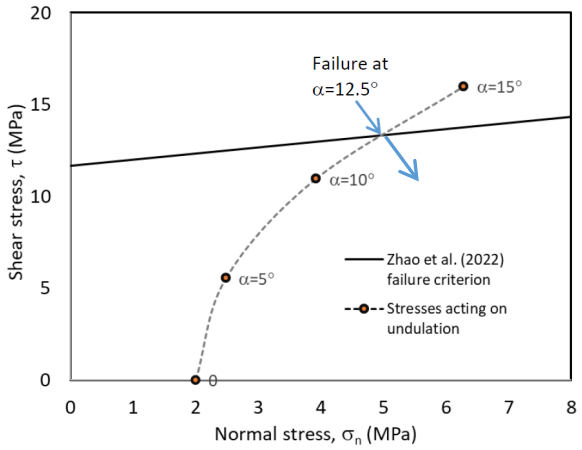

Figure 6. Normal and shear stresses acting on segments of bedding plane undulations oriented at α from the vertical with σ_1=66 MPa and σ_3=2 MPa compared with the failure criterion of Zhao et al. (2022) for fractures with calcite infilling.

4 CONCLUSIONS

Triaxial shear tests at different confining pressures were carried out on samples of organic-rich Mancos shale to understand the effect of the layered structure of shale on its shear failure and fracturing behavior. The samples were drilled horizontally along the bedding planes and loaded with the major principal stress σ_1 parallel to the bedding planes.

For the test sample at low confining stress, the presence of the bedding planes made the tested shale more brittle by allowing extensional fractures to form along the bedding planes even in the presence of significant non-zero confining stress. The sample with a high confining stress of 12 MPa behaved in a transitional brittle-to-ductile response, with conjugated shear fractures combined with bulging due to the anisotropy from the bedding planes.

A new mechanism was proposed to explain fracturing along bedding planes at significantly high confining stress σ_3 which was perpendicular to the bedding plane. The fracturing was attributed to the failure along the undulating segments of the existing infilled bedding plane fractures. The failure resulted in the dilation and opening of the bedding planes, creating extensional fractures in a compressive environment.

In practice in the field, the type of shear fracturing along the bedding planes due to initial anisotropy shown in this study can be achieved by increasing the horizontal stress σ_h above the constant vertical stress σ_v by pressurizing a borehole. Following pressurization, the vertical stress should become the minimum principal stress σ_3, and the horizontal stress should be σ_1. The proposed fracturing mechanism will also occur regardless of drainage conditions. The wellbore pressure may cause vertical hydraulic fracturing first, while the minimum principal stress σ_3 is still horizontal. However, horizontal fractures along the bedding planes may occur as secondary fracturing.

REFERENCES

Neuzil C.E. 1994. How permeable are clays and shales? Water Resources Res. 30 (2), 145-150

IPCC 2005. *Special Report on Carbon Dioxide Capture and Storage*. Chapter 5. International Panel on Climate Change

Guo C., Wei, M. & Liu, H. 2018. Study of gas production from shale reservoirs with multi-stage hydraulic fracturing horizontal well considering multiple transport mechanisms. *PLoS One*, 13(1), e0188480.

Zhao, Z., Tao L., Chen, Y., Zhao, X., Chen, L. & Wang, J. 2022. Shear behaviors of natural rock fractures infilled with cemented calcite. *Comp. Geotech*. 14, 104493.